



NUMERICAL MODELING OF GEOLOGIC STRUCTURES USING 2D RESISTIVITY IMAGING WITH SEVEN ELECTRODE ARRAYS

F. J. Ogunmola, S. O. Adetola* and A. D. Olajumoke

Department of Geophysics, Federal University Oye-Ekiti, Ekiti State, Nigeria

*Corresponding author: sheunsky@gmail.com

Received: December 17, 2016

Accepted: March 29, 2017



Abstract: Numerical modeling of geological models was used to compare the resolution and effectiveness of 2D resistivity imaging survey with seven electrode arrays. The arrays used are the pole-dipole (PD), wenner-alpha(WN), wenner-schlumberger (WS), dipole-dipole (DD), wenner-beta (WB), wenner gamma (WG) and multiple gradient (MG). Three synthetic geological models that simulate a buried channel, claylens and sandlens were generated using RES2DMOD software. These models were contaminated with 5% noise level in order to simulate field data. The geological models were inverted using RES2DINV with robust inversion and smoothness-constrained least-squares techniques. The inverted results were examined for image resolution and anomaly effects (AE) were calculated to measure the effectiveness of these arrays. The inversion results showed that the robust inversion gives better imaging resolutions than the smoothness-constrained least-squares inversion. It was also observed that WS is the most effective for imaging a buried channel while DD is the most suitable array for claylens and sandlens. The calculated AE for the different arrays vary with the geological models with DD having the highest value in almost all the models. However, the relative high AE does not coincide with good image resolution from the inversion. This study has determined the resolution and effectiveness of 2D resistivity imaging with seven electrode arrays in resolving three geological models that could be a guide for geophysical field investigation.

Keywords: Claylens, electrode arrays, geological models, sandlens, numerical

Introduction

Modelling is a very important and useful tool in applied geophysics for comparing the resolution power of different direct current (DC) resistivity electrode arrays (Martorana *et al.*, 2009). Numerical modelling is the science of creating computerized representations of portions of the Earth's crust based on geophysical and geological observations made on and below the Earth surface. DC electrical resistivity survey is a very useful geophysical exploration method because of its simple physical principle and efficient data acquisition (Loke and Barker, 1996). Resistivity measurements are carried out on the Earth's surface with specified array in order to obtain apparent resistivity sounding curves, profiling data, pseudosections which all reflect qualitatively the vertical or horizontal variations of the subsurface resistivity (Loke and Barker, 1996). The areas of applications are very wide in groundwater, civil engineering and environmental investigations and they are also employed in 2D or 3D resistivity imaging for environmental studies.

Different electrode arrays have been used in electrical explorations for groundwater, environmental and engineering purposes (Aizebeokhai and Olayinka, 2010; Amidu and Olayinka, 2006). These arrays include wenner alpha (WN), wenner beta (WB), wenner gamma (WG), dipole-dipole (DD), pole-dipole (PD), pole-pole (PP), wenner-schlumberger (WS), multiple-gradient (MG), schlumberger (SC) etc. These arrays provide useful practical options for surface sounding, profiling and scanning surveys in different situations (Aizebeokhai and Olayinka, 2010; Storz *et al.*, 2000). For resistivity imaging, there might be differences in the imaging capabilities of the electrode arrays when applied to a geological model, that is, differences in spatial resolution, in tendency to produce artefacts in the images, in deviation from the true model resistivity and in interpretable maximum depth (Aizebeokhai and Olayinka, 2010; Dahlin and Zhou, 2004).

In this study, we investigated the behaviours of seven electrode arrays for imaging three synthetic models (buried channel, claylens and sandlens), which are intended to reflect some geological structures in practice.

Significance of the Geological Structures

Buried channel

Buried channel can be referred to as a remnant of an inactive river or stream channel that has been filled or buried by younger sediments. It can also be explained as an abandoned

erosional feature and, along the channel, one can expect fined coarsely granular bed-load stream deposits (Anand and Paine, 2002; Douglas *et al.*, 2003). Buried channel help to aid in understanding movements of faults, which may redirect river systems. It also helps in estimating the net erosional budget of older regolith. Buried channel host economic ore deposits such as uranium, lignite, precious stone, metals etc. It serves as good site for ground water accumulation. It can pose a leakage problem under a dam (Anand and Paine, 2002; Douglas *et al.*, 2003).

Sandlens

Sandlens is a body of sand with the general form of a lens, thick in the centre part and thinning towards the edges. It can also refer to an irregular shaped formation consisting of a porous and permeable sedimentary deposit surrounded by impermeable body. Sandlens serve as a permeable and porous layer/formation for storability and transmissivity of water; i.e. it can serve as aquifer for water accumulation.

Claylens

Claylens is a layer made up of clay particles which can protect groundwater by stopping or preventing movement of contaminants through it. It is a body of clay with a thick middle and thin edges. It serves as a confining layer/formation for an aquifer; it is a protective layer for groundwater. It is a good site for earthling.

Materials and Methods

Synthetic Models

To determine the imaging capabilities of the electrode configurations, three (3) geometries representing various geological models were designed (Fig. 1). The first model is a buried channel (Fig. 1a) of coarse-grained sediments with 5.0 m thick overlying layer of resistivity 600 Ω m. This upper layer rests on the layer of 50 Ω m and has an embedded trapezoidal structure of resistivity 150 Ω m reaching a maximum depth of 15 m. Geologically, it could be a simplified model of an old river channel in a clay environment which has been covered by lateritic sediments. The second model is a claylens model (Fig. 1b) consisting of a 24 m wide claylens of resistivity 50 Ω m in a host layer of sandy sediment with resistivity 250 Ω m. The third model is a sandlens model (Fig. 1c) consisting of a 24 m wide sandlens of resistivity 250 Ω m in a host layer of clayey sediment with resistivity of 50 Ω m.

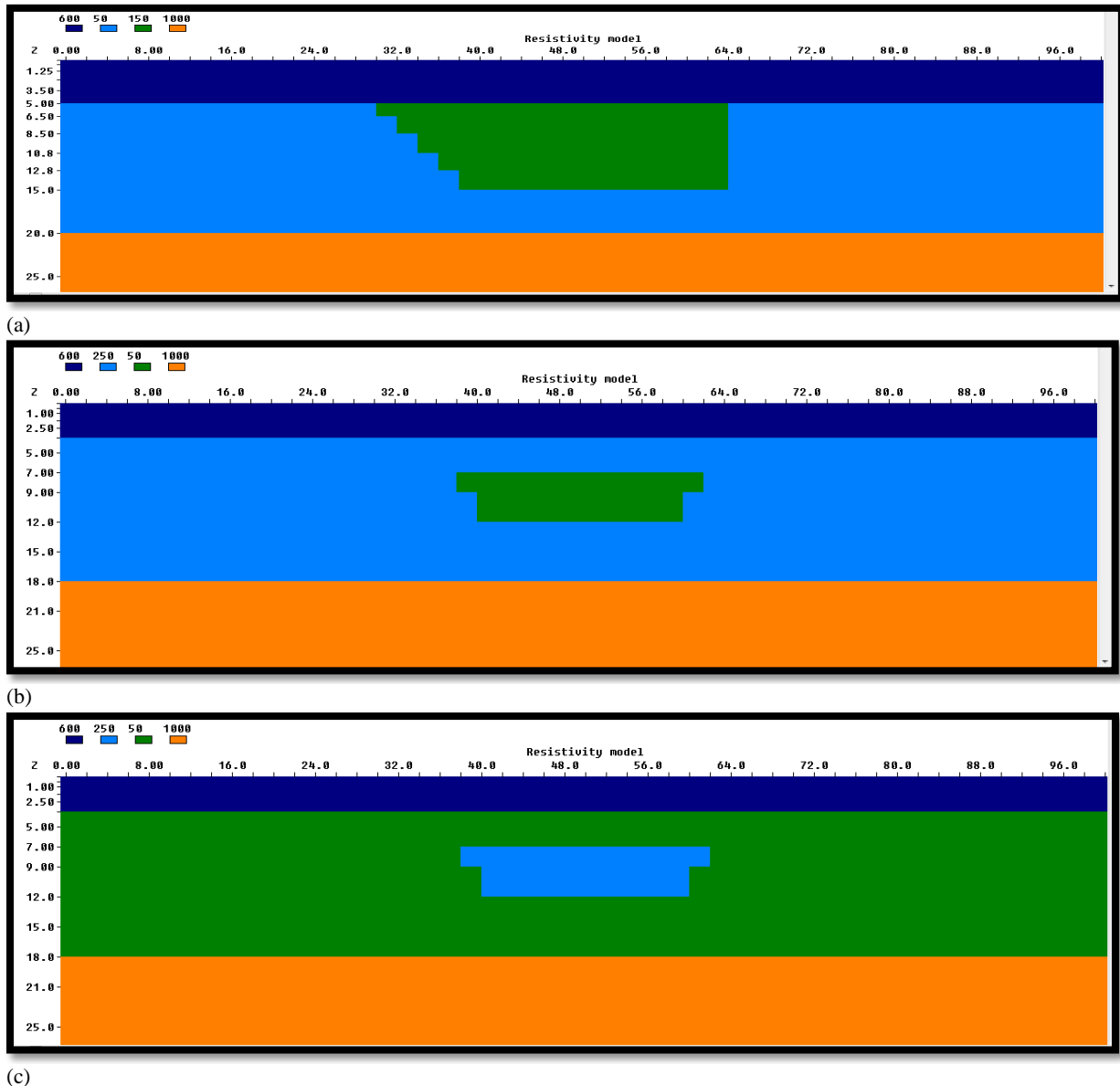


Fig. 1: Synthetic models for numerical imaging experiments (a) A simplified model of an old river channel in a clayey environment (b) A claylens model (c) A sandlens model

Determination of apparent resistivity and measurement of effectiveness

Synthetic apparent resistivity data were generated over resulting set of 2D profiles using RES2DMOD forward modelling code for selected arrays (Loke, 2000). Electrode layout with separation, $a=2$ m, and $L=100$ m were used. The resistivity of each model was allowed to vary arbitrarily along the profile and with depth. Finite difference method (Dey and Morrison, 1979) which determines the potentials at the nodes of the rectangular mesh was employed in the calculation of the potential distribution. The calculated apparent resistivity values were contaminated with 5% Gaussian noise (Press *et al.*, 1996) so as to stimulate field conditions (Dahlin and Zhou, 2004). The apparent resistivity data computed for the series of 2D models were inverted using RES2DINV inversion software (Loke and Barker, 1996). The number of electrodes in each 2D profile, number of profiles collated and their directions determine the size and pattern of the electrode grid obtained. Two popular inverse schemes; robust inversion and smoothness-constrained least squares inversion were

applied and a comprehensive comparison of all the electrode arrays for 2D resistivity imaging was made.

The anomaly effect (AE) developed by Milner *et al.* (1979), is usually used to evaluate the effectiveness of the resistivity measurements of the electrode array. From imaging point of view, the value of the AE should be significantly greater than the background noise for an effective survey. Therefore, the anomaly effect of the electrode arrays on the three geologic models was used in determining the array(s) with better resolution and sensitivity. The 2D apparent resistivity values were assessed and used to estimate the anomaly effects of the arrays on the synthetic models. The mean absolute anomaly effects on the models for a given electrode configuration is defined in equation (1). According to Dahlin and Zhou (2004), arrays with high anomaly effects yield inversion images with better resolution and model sensitivity than arrays with low anomaly effect and its varies from geological model to geological model depending on the resistivity contrast and general background noise level.

$$AE = \frac{\rho_{max} - \rho_{min}}{\rho_{av}} \quad (1)$$

Where: ρ_{max} , ρ_{min} , and ρ_{av} are maximum, minimum and average apparent resistivities respectively, observed for electrode configuration.

Results and Discussion

Buried channel

The inversion for buried channel is presented in Figs. 2a-n obtained with smoothness constraint and robust inversion techniques. From the results, it was observed that WS produced better resolution than others although the array exaggerated the thickness of the feature as seen in Figs. 2a-b. WG (Figs. 2c-d) and MG (Figs. 2e-f) also imaged the feature with better resolution although MG also exaggerated the thickness a little but not as high as that of WS. WG also

reduced the thickness of the original model from 10 m to 9.89 m with a fair resolution of the image. WN and WB have a fairly good image resolution but neither of them mapped the trapezoidal shape of the target as well as WS, MG, WG and DD. DD and PD gave poor resolution as both did not image the geological feature as others. It was observed that the robust inversion technique gave better resolution than smoothness constraint for most of the arrays. This may be because robust inversion attempts to find a model minimises the absolute values of the data misfit, and the smoothness seeks a smooth model that minimises the squares of data misfit (Dahlin and Zhou, 2004).

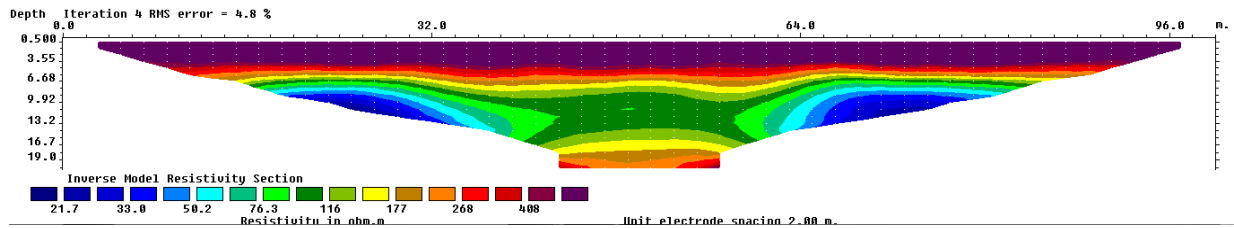


Fig. 2a: Smoothness constraint inversion-WS of buried channel

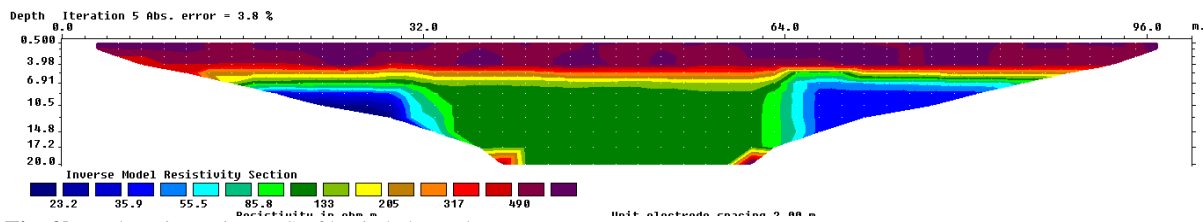


Fig. 2b: Robust inversion-WS of buried channel

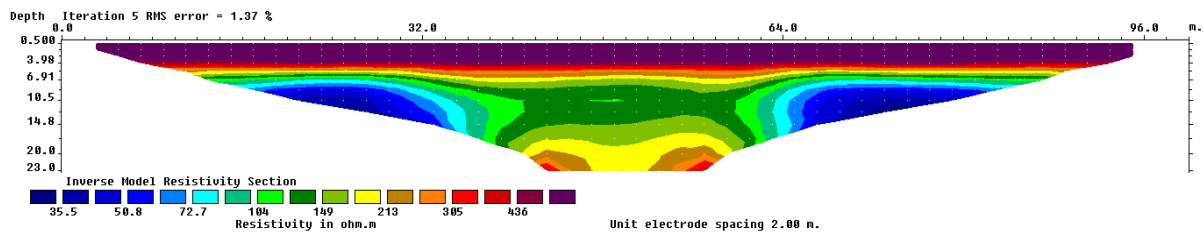


Fig. 2c: Smoothness constraint inversion-MG of buried channel

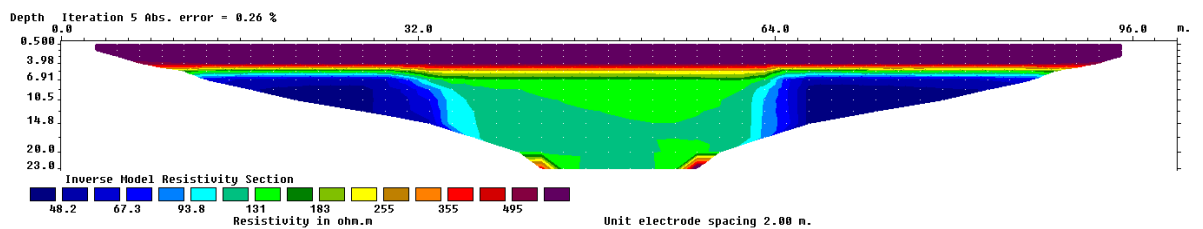


Fig. 2d: Robust inversion-MG of buried channel

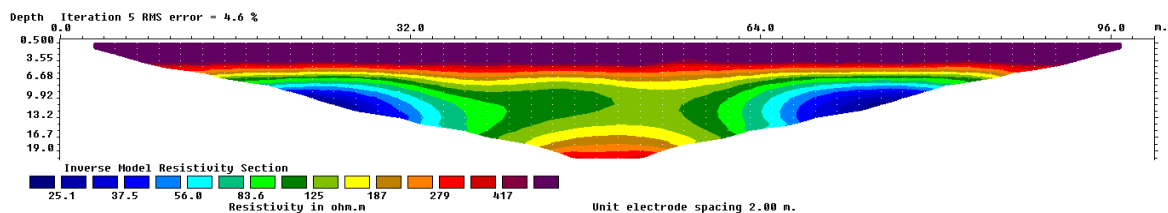


Fig. 2e: Smoothness constraint inversion-WG of buried channel

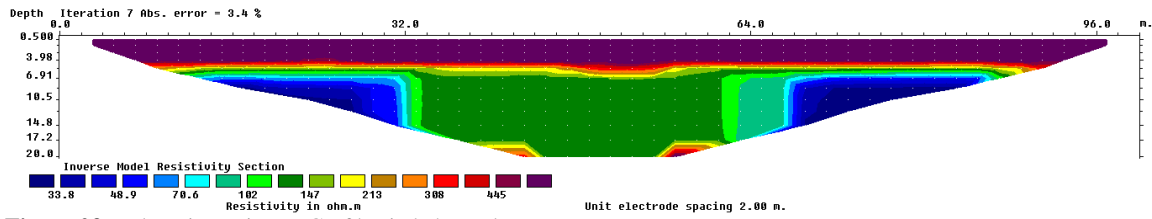


Figure 2f: Robust inversion-WG of buried channel

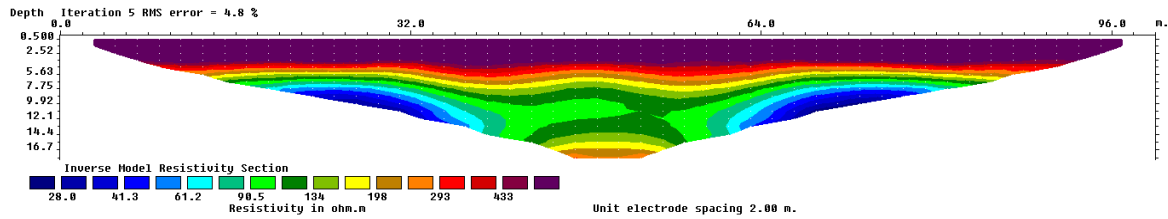


Fig. 2g: Smoothness constraint inversion-WN of buried channel

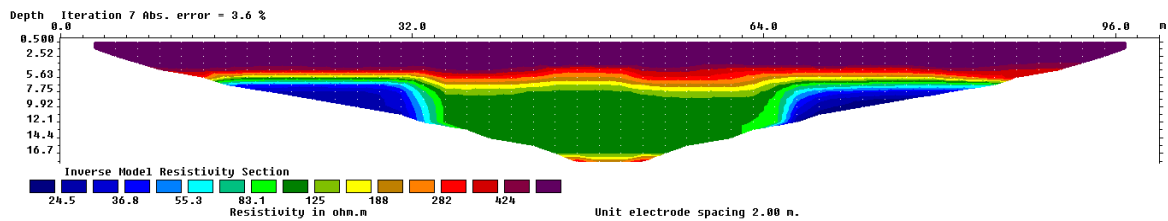


Fig. 2h: Robust inversion-WN of buried channel

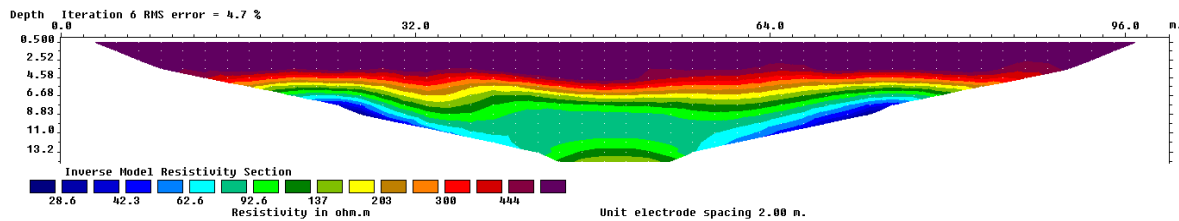


Fig. 2i: Smoothness constraint inversion-WB of buried channel

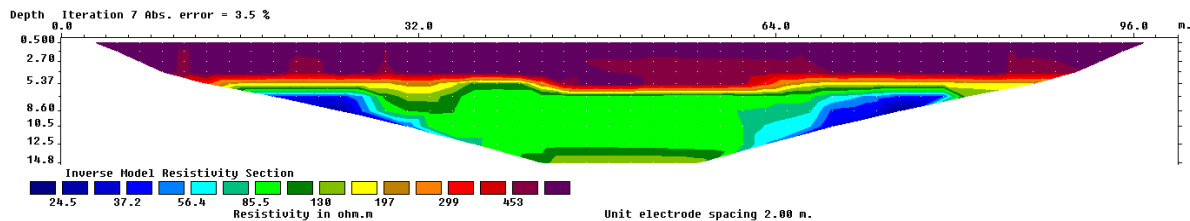


Fig. 2j: Robust inversion-WB of buried channel

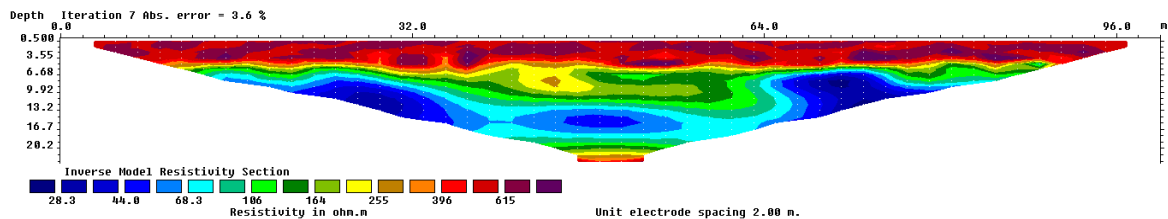


Fig. 2k: Smoothness constraint inversion-DD of buried channel

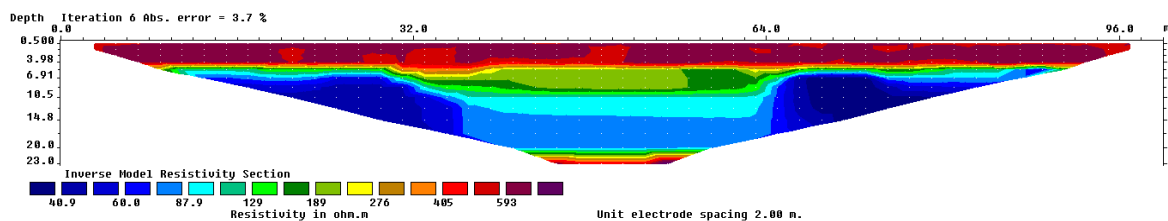


Fig. 2t: Robust inversion-DD of buried channel

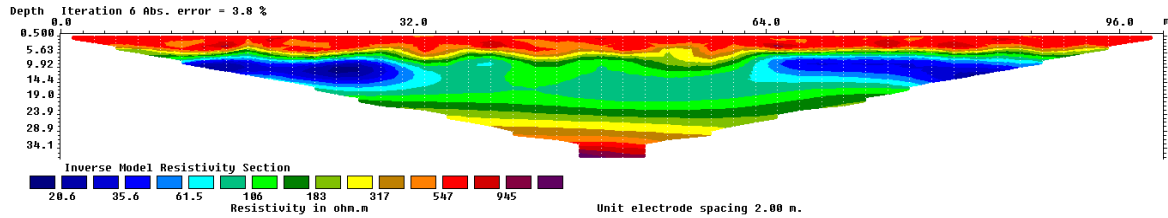


Fig. 2m: Smoothness constraint inversion-PD of buried channel

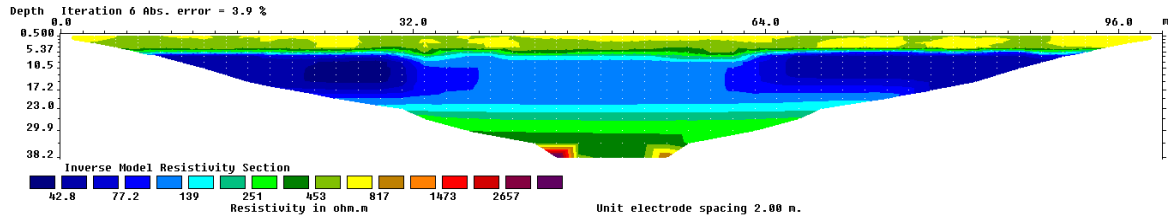


Fig. 2n: Robust inversion-PD of buried channel

The variation of the calculated anomaly effects of the different electrode arrays for buried channel is shown in Fig. 3. It was observed that the AE are ranked as DD, PD, WB, WS, WN, MG and WG with DD being the array with the highest and WG the least. The implication of this is that DD with highest AE should produce the best image with best resolution. Meanwhile, the inversion result of the model gave WS and MG as the arrays with best resolution.

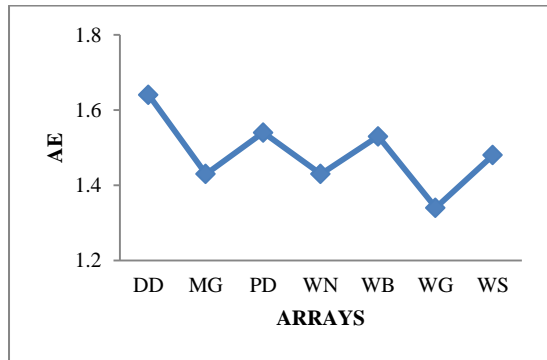


Fig. 3: AE variation for buried channel

Claylens

Figures 4a-n shows smoothness and robust inversion result of the claylens. The result shows that all the arrays depicted the image with DD, MG and PD having the best resolution and produced the best image for the claylens model (Figs 4a-f). However, it was noted that DD and MG exaggerated the lateral extent of the feature. WB, WG and WS (Figs 4g-i) also produced better image with good resolution though the WB using robust inversion exaggerated the thickness of the feature and WG exaggerating the lateral extent of the model. However, WN (Figs. 4m-n) produced a good resolution of the image but there exist a shadow zone of resistivity beneath the target.

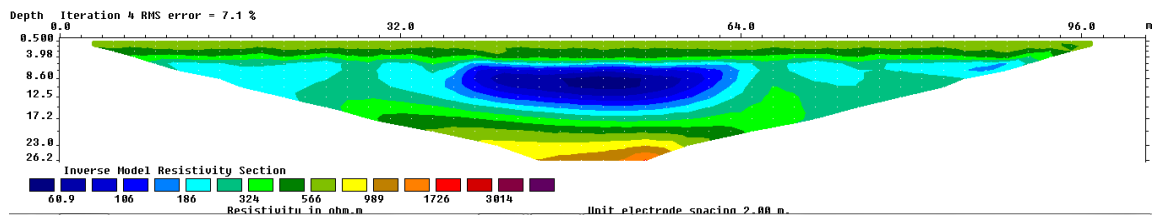


Fig. 4a: Smoothness constraint inversion-DD of claylens

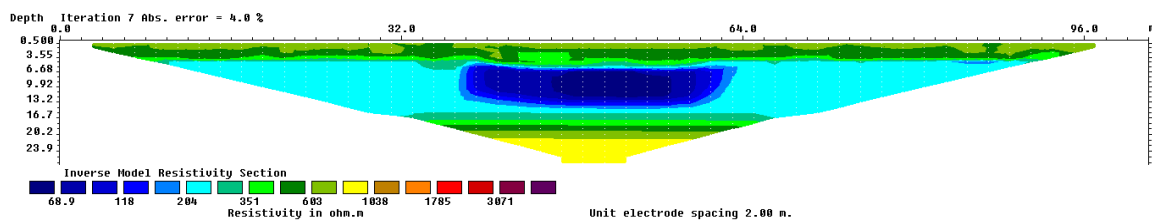


Fig. 4b: Robust inversion-DD of claylens

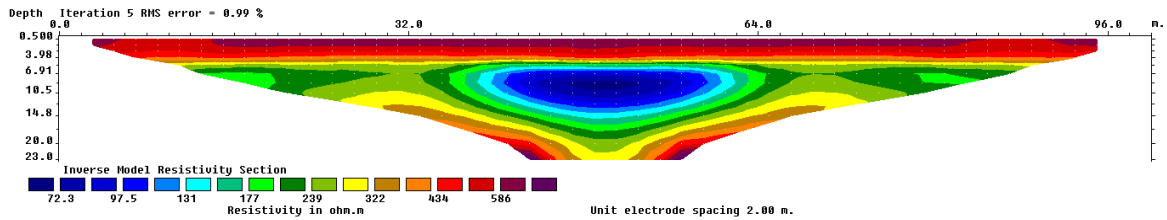


Fig. 4c: Smoothness constraint inversion-MG of claylens

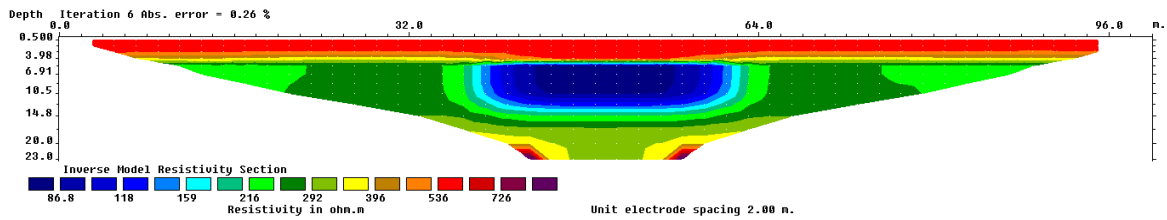


Fig. 4d: Robust inversion-MG of claylens

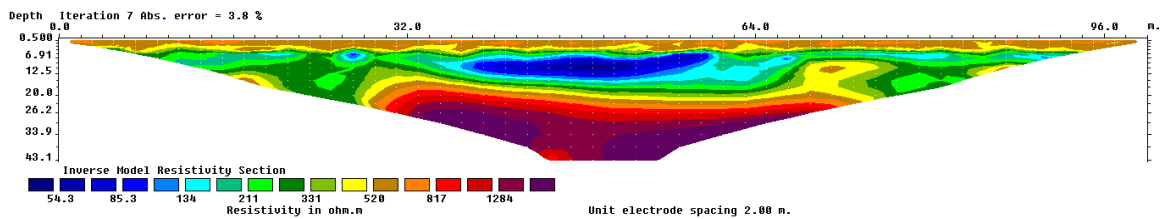


Fig. 4e: Smoothness constraint inversion-PD of claylens

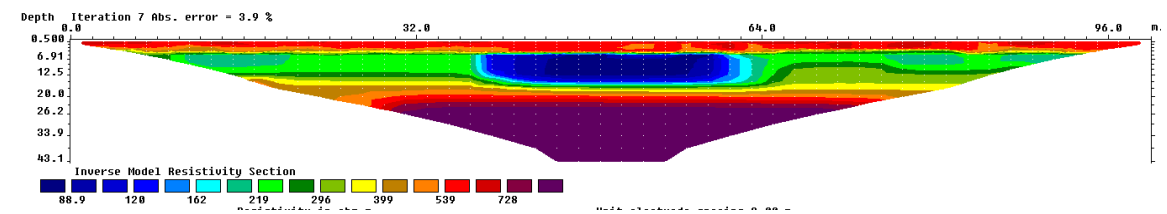


Fig. 4f: Robust inversion-PD of claylens

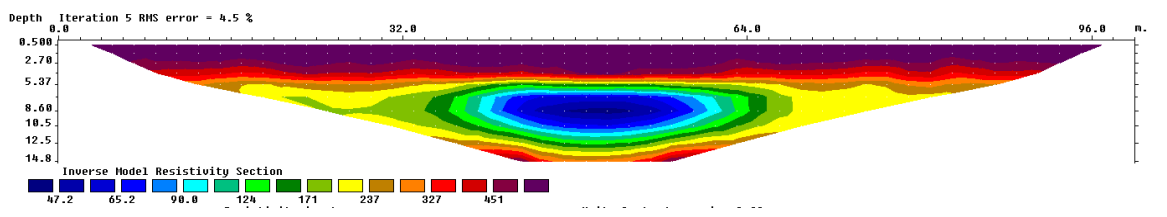


Figure 4g: Smoothness constraint inversion-WB of claylens

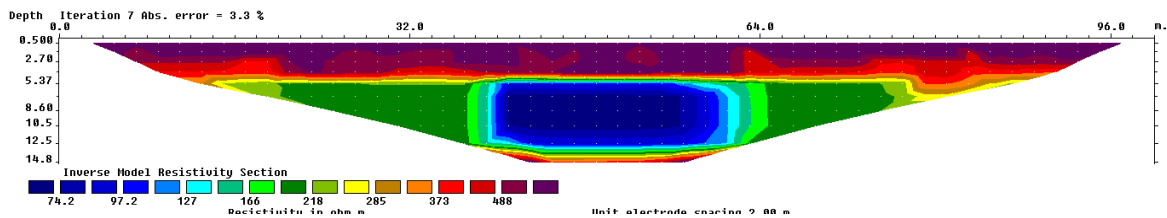


Fig. 4h: Robust inversion-WB of claylens

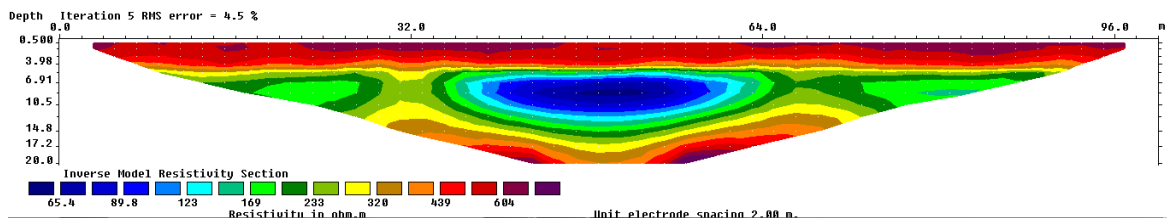


Fig. 4i: Smoothness constraint inversion-WG of claylens

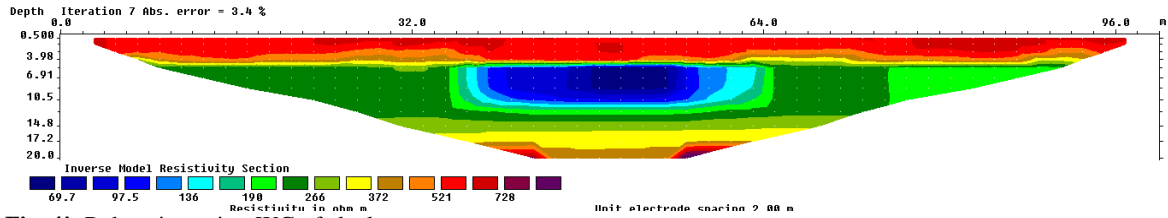


Fig. 4j: Robust inversion-WG of claylens

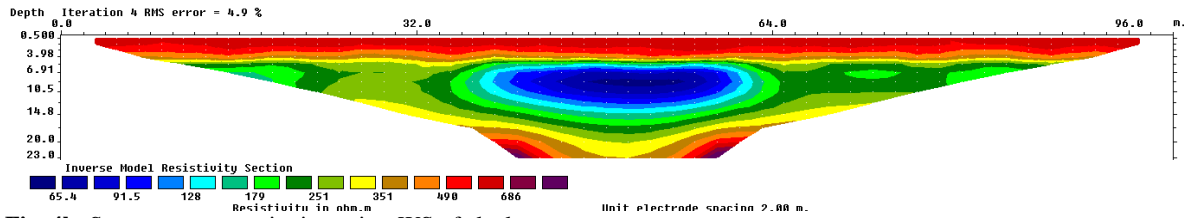


Fig. 4k: Smoothness constraint inversion-WS of claylens

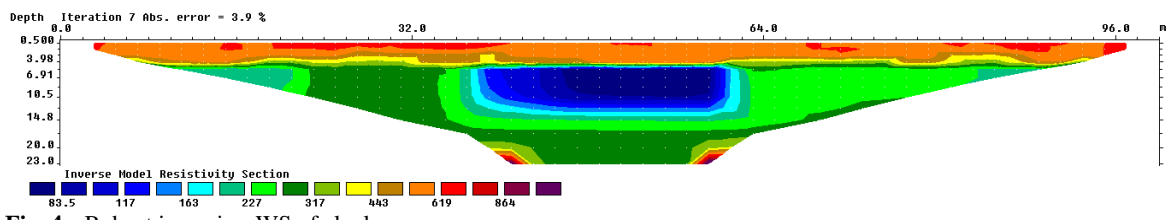


Fig. 4l: Robust inversion-WS of claylens

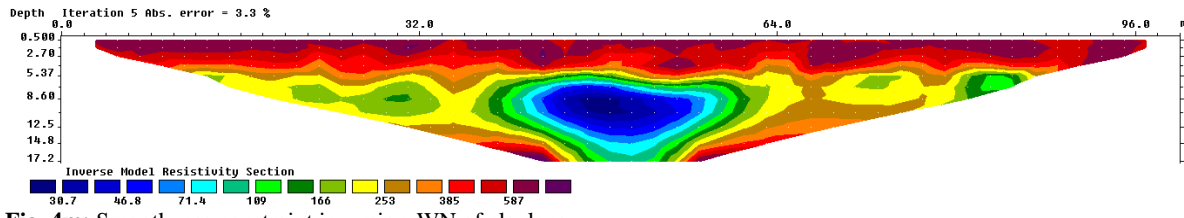


Fig. 4m: Smoothness constraint inversion-WN of claylens

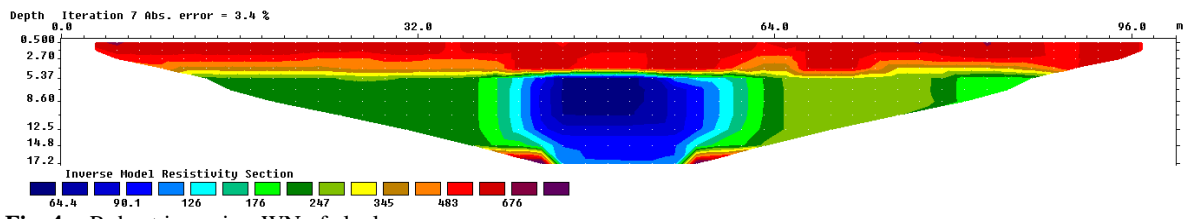


Fig. 4n: Robust inversion-WN of claylens

The variation of calculated AE for different arrays in claylens is shown in Fig. 5. Here, the result shows that DD has the highest AE then PD, followed by WB and WS then WN, WG and MG having the least AE. This implies that using AE for the effectiveness of electrode arrays, DD is expected to produce image with best resolution. However, the inversion result of the model gave DD, MG and PD as the arrays with best resolution.

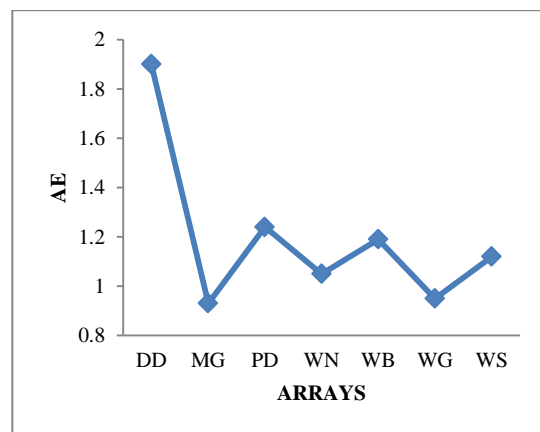


Fig. 5: AE variation for claylens

Sandlens

The inversion results for the modelled sandlens are presented in Figs. 6a-n. It is seen from the result that DD and PD (Figs. 6a-d) have the best resolution and best image of the feature than the other arrays. WS (Figs. 6e-f) appears to have lesser resolution and image compared to that of DD and PD while MG, WB, WG and WN have no clear image for the feature as seen in Figs. 6g-n.

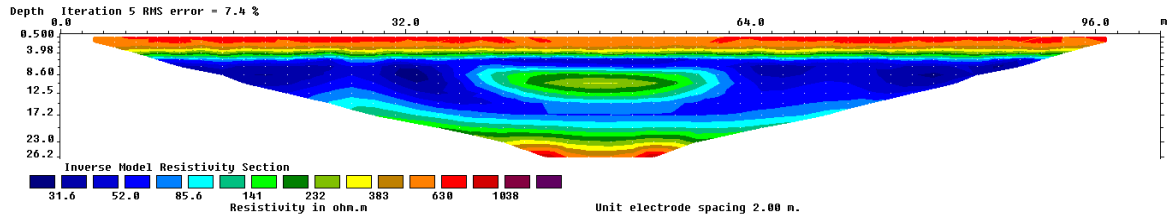


Fig. 6a: Smoothness constraint inversion-DD of sandlens

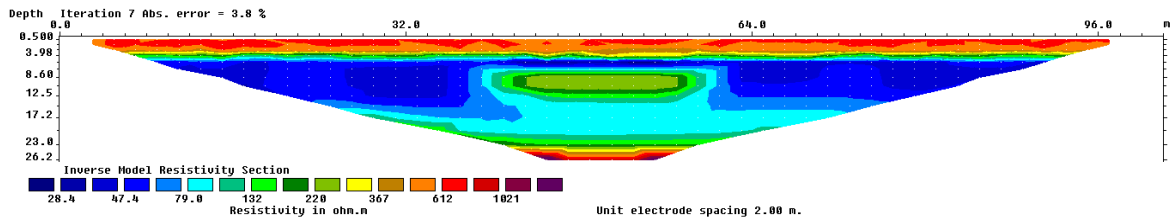


Fig. 6b: Robust inversion-DD of sandlens

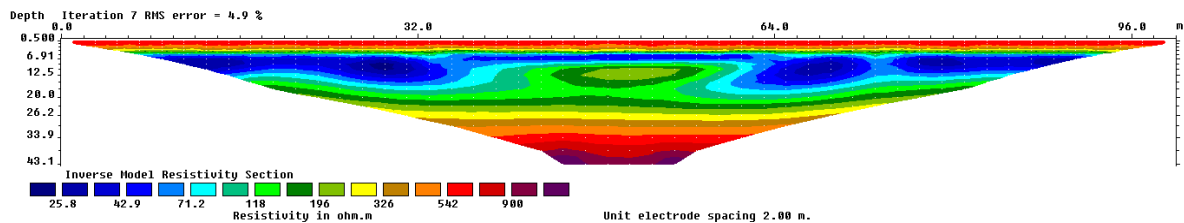


Fig. 6c: Smoothness constraint inversion-PD of sandlens

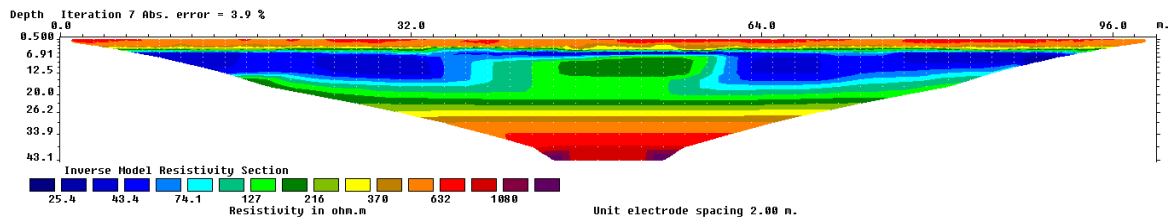


Fig. 6d: Robust inversion-PD of sandlens

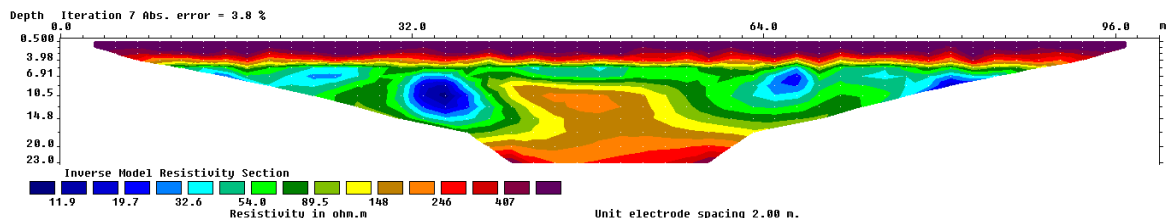


Fig. 6e: Smoothness constraint inversion-WS of sandlens

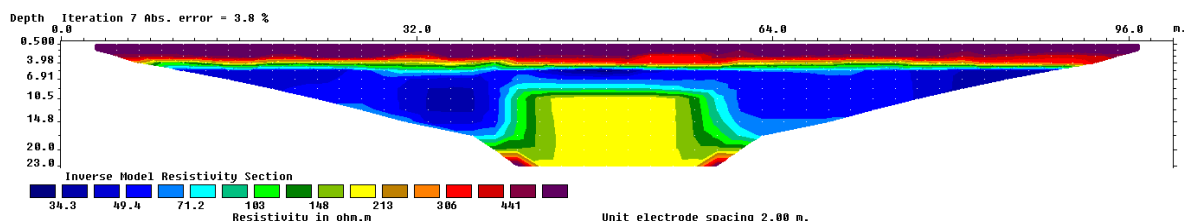


Fig. 6f: Robust inversion-WS of sandlens

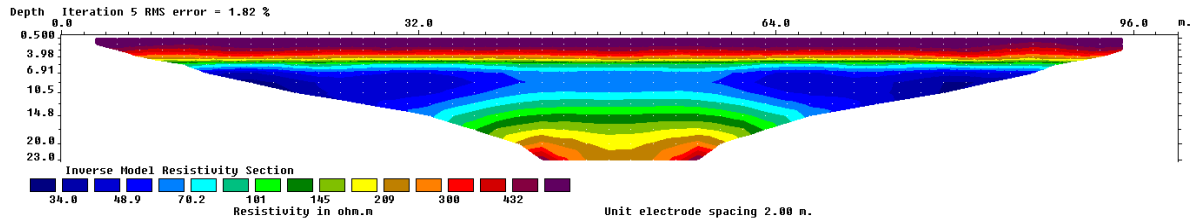


Fig. 6g: Smoothness constraint inversion-MG of sandlens

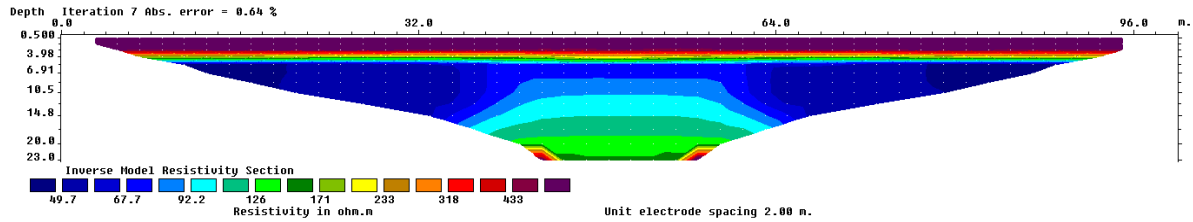


Fig. 6h: Robust inversion-MG of sandlens

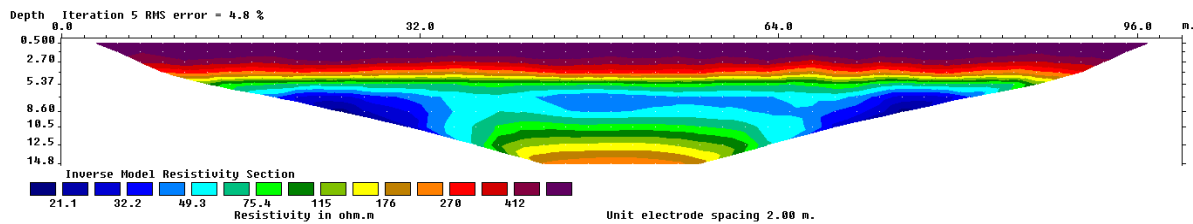


Fig. 6i: Smoothness constraint inversion-WB of sandlens

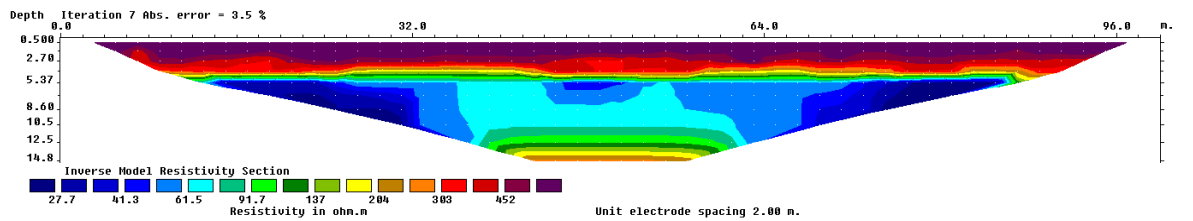


Fig. 6j: Robust inversion-WB of sandlens

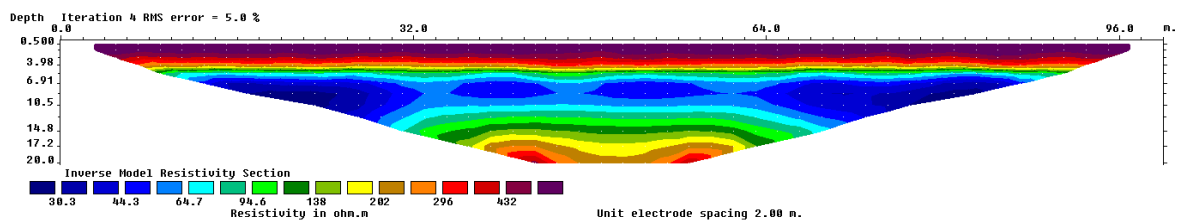


Fig. 6k: Smoothness constraint inversion-WG of sandlens

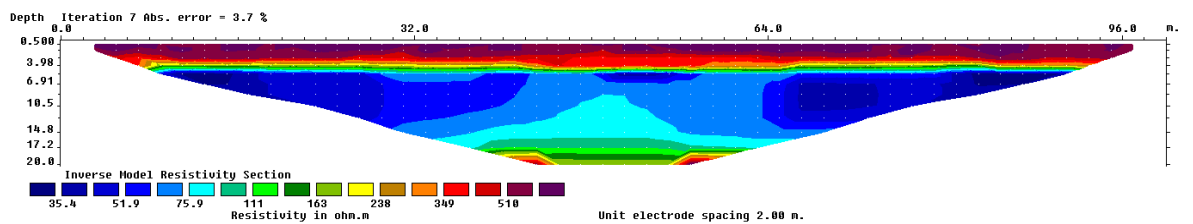


Fig. 6l: Robust inversion-WG of sandlens

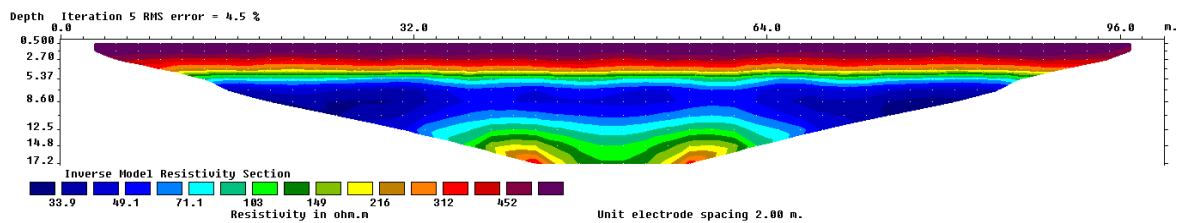


Fig. 6m: Smoothness constraint inversion-WN of sandlens

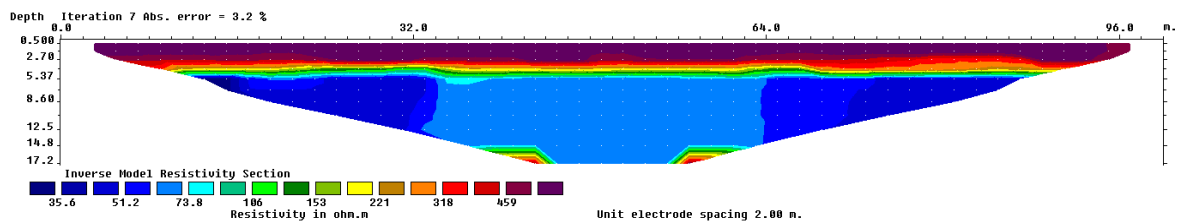


Fig. 6n: Robust inversion-WN of sandlens

The variation of AE in sandlens is shown in Fig. 7. It is observed from the result that DD and WB have the highest AE and following these arrays are PD, WS, WN, and MG having the least AE. DD and WB are expected to be very effective in producing images with best resolutions while MG should produce images with poor resolution. Other arrays such as PD, WS and WN are expected to yield images with fairly good resolution based on their values of AE. Conversely, the inversion results show that DD and PD produced images with the best resolution and WS yielded a fairly good resolution while all other arrays MG, WB, WG, and WN gave no clear image of the feature.

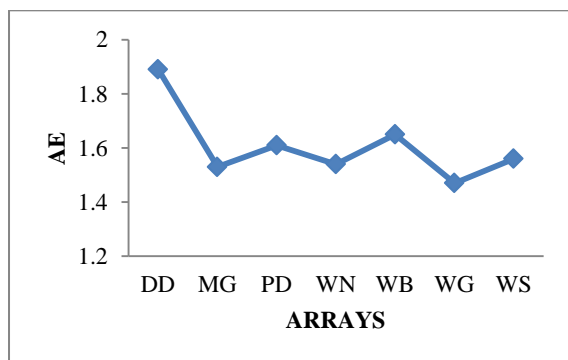


Fig. 7: AE variation in sandlens.

From the results it can be seen that high AE does not necessarily coincide with the resolution. However, the claylens shows a level of correlation between resolution of image from the inversion result and the AE results as the best resolution came from the DD array and the highest AE is also the DD, and MG with the least AE is observed to give the second best resolution.

Conclusion

The numerical modeling of three synthetic models; buried channel, claylens and sandlens was done in order to assess the effectiveness of electrode arrays in resolving geological structures. This was done by both forward modelling and inversion. The forward modeling was done using RES2DMOD software by Loke. The inversion of these models was carried out using RES2DINV involving two techniques; the smoothness constraint and the robust inversion techniques. A measure of effectiveness of the arrays

was employed by calculating the anomaly effects of each array.

It was obtained from the result that, for buried channel; WS has the best resolution with DD giving the least resolution and the anomaly effect show DD as having the highest anomaly effect value and WG ranking the least. For claylens DD, MG, PD have the best resolution with the other arrays having moderately good resolution, DD and PD gave the highest anomaly effect value and WG and MG have low anomaly effect. Finally, for sandlens the result shows that only three electrode arrays (DD, PD and WS) were able to image the feature with two of them (DD and PD) having a better resolution than that of WS. The other arrays have no visible image. WS is the most suitable for buried channel while DD, MG and PD are the most effective arrays to image any claylens while DD, PD and WS are very effective for imaging sandlens.

From this study, it was realised that high AE of some arrays does not necessarily coincide with high resolution image. However, the aforementioned arrays suitable for each synthesized geological structures and features should be tested with field data.

References

- Aizebeokhai A P & Olayinka AI 2010. Anomaly effects of arrays for 3D geoelectrical resistivity imaging using orthogonal or parallel 2D profiles. *Afri. J. Envntal. Sci. & Techn.*, 4(7):446-454.
- Amidu SA & Olayinka AI 2006. Environmental assessment of sewage disposal systems using 2D electrical resistivity imaging and geochemical analysis: A case study from Ibadan, Southwestern Nigeria. *Envnt. Engr. Geosci.*, 7(3): 261-272.
- Anand RR & Paine M 2002. Regolith geology of Yilgarn Craton, Western Australia: Implications for exploration. *Australian J. Earth Sci.*, 49(1):3-162.
- Dahlin T & Zhou B 2004. A numerical comparison of 2D resistivity imaging with 10 electrodes array. *Geophysical Prospecting*, 52: 379-398.
- Dey A & Morrison HF 1979. Resistivity modeling for arbitrarily shaped two-dimensional structures. *Geophysical Prospecting*, 27:106-136.
- Douglas GB, Butt CRM & Gray DJ 2003. Mulga rock uranium and multielement deposits, officer Basin, WA. Report of CRC for Landscape Evolution and Mineral Exploration, <http://leme.anu.edu.au>.

The Use of Numerical Modeling of Geological Models Structures

- Loke MH & Barker RD 1996. Rapid least-squares inversion of apparent resistivity pseudosections by a quasi-Newton method. *Geophysical Prospecting*, 44: 131-152.
- Loke MH 2000. Electrical imaging surveys for environmental and engineering studies. *A practical guide to 2-D and 3-D surveys*, www.geo.mtu.edu.
- Martorana R, Flandaca G, Ponsati AC & Cosentino PL 2009. Comparative tests on different multi-electrode arrays using models in near surface geophysics. *J. Geophysics & Engr.*, 6(1):1-9.
- Militer H, Rosler R & Losch W 1979. Theoretical and experimental investigations of cavity research with geoelectrical resistivity methods. *Geophysical Prospecting*, 27: 640-652.
- Press WH, Teukolsky SA, Vetterling WT & Flannery BP 1996. Numerical recipes in Fortran 77: The Art of Scientific Computing, Volume 1, 2ndedn., Cambridge University Press, p. 1003.
- Storz H, Storz W & Jacobs F 2000. Electrical resistivity tomography to investigate geological structures of the earth's upper crust. *Geophysical Prospecting*, 48(26): 455-471.